JOURNAL OF AIRCRAFT
Vol. 33, No. 1, January–February 1996

Modified, Discrete-Vortex Method for Studying Wing-Loading Effects on Wake Dynamics

V. R. Nikolic*
Rose–Hulman Institute of Technology, Terre Haute, Indiana 47803
and
E. J. Jumper† and R. C. Nelson‡
University of Notre Dame, Notre Dame, Indiana 46556-5637

An inviscid model for calculating the roll up of wing-generated, vortical wakes has been developed. The model is shown to be an efficient means of studying the dynamics of the wake in the region from just behind the wing to the previscous-dissipation far field. The model is based on a modified discrete-vortex method that includes the near-wing effects of the wing-bound vorticity and the fact that the wake originates at the wing, rather than at minus infinity. Three-dimensional wakes are produced by connecting the two-dimensional wake contours at successive Trefftz planes. The inclusion of the near-wing effects is shown to have a relatively large influence on the wake's dynamics and final disposition. The inclusion of rotational cores is shown to aid in smoothing the wake roll up, but appears to have little effect on the wake's final dispersion radii.

I. Introduction

SINCE the earliest developments in the theory of aerodynamics, it has been known that the production of lift by a wing of finite span is accompanied by a sheet of streamwise vorticity issued from the trailing edge of the wing, whose semispan circulation strength is related to the lift produced by the wing. In the case of a normal, steady, wing-load distribution, this sheet rolls up into two opposite-sense vortices commonly referred to as wingtip vortices, although their centers of vorticity are, in general, less than a span apart. The strength of these wingtip vortices Γ is given by

$$\Gamma = W/\rho V_\infty b' \tag{1}$$

where W is the airplane weight, ρ is the air density, V_∞ is the airspeed, and b' is the distance between the trailing vortices or the vortex span. It can be seen from Eq. (1) that the strongest vortices occur during takeoff and landing when, in the first case, the aircraft weighs the most, and in both cases, the airspeed is the least. These wingtip vortices are known to pose a hazard to following aircraft, where, depending on vortex strength, the relative trajectories of the vortices, and the penetrating aircraft, moments can be imposed on the following aircraft sufficient to overwhelm its control capability.[1-3] This hazard poses the greatest threat to safety during landing and takeoff, not only because the strengths of vortices are greatest, but also because aircraft must share common corridors and the near vicinity to the ground and low speed allow little margin for recovery; the introduction of jumbo jets in the early 1970s elevated wake turbulence to a major airport safety issue. Since that time, considerable effort has been directed toward the understanding, measurement, and possible alleviation of the wake-turbulence hazard.[1-8] These efforts (as well as early work by Betz[9] and others) have led to a fundamental understanding of the wake roll-up physics, and at least one known mechanism for an instability driven destruction of the wake.[10,11] Further, the efforts have led to a general understanding of the potential hazard of wakes as functions of the generating and penetrating aircraft, and have led to safe separation criteria for landing and takeoff[2,3]; however, evolution in aircraft designs may have made the categorization of aircraft into specific groups by weight alone less appropriate.[3]

Efforts to directly influence the roll up of the wake by modifying the flowfield at the wing to alleviate the wake hazard have also been undertaken; such direct intervention approaches are referred to as technical solutions. To date, efforts at discovering practical and reliable technical solutions have been illusive[8,12,13]; yet, such technical solutions to the wake-turbulence problem are of interest because the now, Federal Aviation Administration (FAA)-regulation-imposed, safe-separation criteria have a direct impact on airport capacity.[14] The reader is directed to Ref. 8 for an excellent summary of many of the wake-turbulence attenuation schemes proposed and tested up to 1991. Rossow divides these schemes into three categories: 1) viscosity and turbulence generators to hasten viscous decay; 2) small-scale, vortex-instability initiators; and 3) large-scale, vortex-instability initiators. Methods investigated that fall into the first two categories have either been shown to be ineffective or impose unacceptably high drag penalties when the wake-turbulence hazard is reduced. On the other hand, large-scale vortex instability generators have been shown to be successful in alleviating the wake hazard; however, in some cases, landing gear and ground effect have made schemes ineffective that may otherwise have shown promising results. These large-scale effects have been achieved by modified wing loads (e.g., flap deflection schedules) and by injecting vortices into the wake at, but out of plane with, the wing. These large-scale, vortex-instability schemes have been identified by NASA as promising avenues for future research, but to date, the reason for their effectiveness is not understood. The common factor involved in the successful large-scale, vortex-instability schemes appears to be that they involved inviscid vortex interactions in the near-field wake (i.e., just behind the wing) out to the relatively near, far-field wake.

Our research has been directed toward contributing to the understanding of why some of these large-scale, vortex-insta-

Received July 19, 1993; revision received Oct. 10, 1994; accepted for publication Aug. 23, 1995.

*Assistant Professor, Department of Mechanical Engineering. Member AIAA.
†Associate Professor, Department of Aerospace and Mechanical Engineering. Associate Fellow AIAA.
‡Professor, Department of Aerospace and Mechanical Engineering. Associate Fellow AIAA.

bility schemes work and others do not. We attempted to gain this understanding by studying the results of computations focused specifically on the near-field to relatively near, far-field dynamics of the developing wake.[15] This article describes our principal tool in the work: a modified, discrete-vortex method for computing the wake as it emanates from a lift-generating wing, deforms and develops its asymptotic character into the previscous-dissipation far field, or near far field.

Our research depended on the acquisition or the development of a computational tool that was efficient (i.e., a large number of input load distributions could be considered) and met the input/output requirements of our studies. Since our studies would be limited to the inviscid dynamics of the wake in the near field to the near far field, Navier–Stokes-type solvers were not applicable and many other computational approaches to the problem could be eliminated. For example, an extensive modular code developed by Continuum Dynamics, Inc., while treating the connection between the wing geometry and the generation of spanwise and streamwise vorticity at the wing, and treating the far field, including viscous dissipation, specifically bypassed the initial, near-field wake dynamics by using a Betz roll-up method.[16] We also considered using a paneling method[17] or a Euler solver; however, these classes of codes require well-defined boundary conditions that require detailed wing-geometry information. Euler codes are also sensitive to proper generation of grids and require preconditioning to make modifications in the load distribution. Further, for our studies the wing load was to be considered an input variable; in both paneling and Euler codes the wing load is a consequence of wing geometry and, as such, not able to be manipulated directly. On the other hand, several wake-vortex studies employed discrete-vortex methods to analyze wake dynamics,[18–20] and for the purposes of our work, this approach seemed most applicable. These methods also exhibit good computational efficiency because of the gross simplification of the flowfield into a two-dimensional mapping of discrete-vortex trajectories computed at each successive Trefftz plane in the wake. Although many discrete-vortex codes have been developed by various researchers, no specific code was available for our use, and, because our focus was on the near- to near far-field dynamics, the fact that no previous studies had included the effect of the initial near vicinity of the wing (i.e., the wing-bound vorticity and the fact that the wake vortices emanate from the wing rather than at $-\infty$) required that we construct our own code. As will be shown later, modeling the near-wing effects had an influence on the ultimate disposition of the wake.

II. Code Requirements

A. Input Requirements

The code described in this article was the consequence of a number of narrowly defined requirements. First, as described in Sec. I, we were interested only in the dynamic evolution of the wake in the near and near far field as influenced by the bound spanwise vorticity at the wing and the shed streamwise vorticity in the wake. On the other hand, we were not interested in detailed spanwise and chordwise load distributions; we viewed the wing as simply a spanwise load (vorticity) distribution; the details of how such a distribution might be formed were not considered other than making use of distributions derived by other methods as a possible input for our study. From a wake-dynamics point of view, the load distribution was to be considered an input variable and the wake dynamics the output variable. As such, we wanted to be able to modify the input load distribution at the wing with little to no code preconditioning.

B. Output Requirements

In studying the evolution of the wake we wanted to track spatial details of the vorticity distribution, as well as the gross parameters (computed from the vorticity distribution) of the first and second semispan moments of vorticity (as well as moments for less-than-full-semispan, well-identified portions of the wake) as a function of distance downstream from the generating wing.

The first and second semispan moments of vorticity were useful in accessing the accuracy of the code, as will be shown; but, they have also been used in the past to determine the merit of given load distributions and/or vortex-injection schemes as wake-turbulence alleviators. The first moment of vorticity (based on the spanwise distance y) when divided by the wake semispan circulation gives the spanwise center of vorticity $y_{c.v.}$, the distance between the left and right $y_{c.v.}$ being the vortex span b' in Eq. (1). Betz was the first to show that $y_{c.v.}$ is invariant with distance from the generating wing,[9] which provides an output variable that is useful in assessing the accuracy of the code. Beyond this, an effective instability for destroying the wake is that explained by Crow[10] and now referred to as the Crow instability. Crow showed that when a sinusoidal disturbance of a most unstable wavelength is imposed on the wingtip vortex pair (either through random perturbations or by design), the wingtip vortices amplify the disturbance and eventually link, turning the wake into a series of vortex rings that no longer poses a safety hazard on a following aircraft. Crow[10] also showed theoretically, and Eliason[11] confirmed experimentally, that b' is a critical factor for the natural development of the instability and breakdown of the trailing vortices (i.e., the time necessary to amplify the disturbance grows as $1/b'^2$).

The semispan second moment of vorticity (based on the absolute distance from the center of vorticity), when divided by the semispan circulation and the square root taken, gives the dispersion radius r_D, a measure of the tightness of the wake roll up. This moment changes with distance from the wing, but, for a normal wing-load distribution, eventually asymptotes to some value; once that value is attained, the wake may be considered to be fully developed, marking the beginning of the near far field. For the usual Oseen-type vortex,[21] a plot of tangential velocity vs radius taken through one of the wingtip vortices starts at zero at the center of vorticity and increases to approximately the edge of the vortex core, then folds over to a $1/r$ decay outside the core. Circulation computed along closed (for convenience) circular paths, of radius r, that completely enclose the core give the circulation strength Γ of the vortex; Γ does not change with r as long as the core is completely enclosed by the path and the path does not contain any other vortices. Therefore, for two vortices of the same circulation, the vortex with the smallest core, and therefore, the smallest second moment of vorticity in the far field, has the largest maximum tangential velocity.

It should be noted that the Oseen-type vortex described earlier has a rotational core. For a discrete-vortex code, the Oseen-type rotational core characteristics may or may not be properly represented by the code. If the vortices are represented by point vortices, then inside the core (that portion of the vortex centered around the center of vorticity, inside of which no vortices are contained) the flowfield exhibits no vortex-associated tangential velocity, whereas outside the core (outside a circular curve centered at the center of vorticity that contains all, and only, those vortices associated with the particular vortex) exhibits essentially a $1/r$-functional, tangential-velocity form. If rotational, singularity cores are prescribed to the discrete vortices for the computational-stability purposes,[22–24] then, depending on the singularity-core radius, the combined vortex core (sum of all discrete vortices) can mimic an Oseen-type vortex. In all cases the dispersion radius is generally prescribed as the nominal radius of the core.[25,26] Further, regardless of the character of the core, when comparing two vortices with the same prescribed rotational-singularity-core character, the vortex with the smallest core (in the far field), and therefore, the smallest second moment of vorticity, has the largest maximum tangential velocity. Because of this inverse

relationship between core radius and maximum tangential velocity, schemes that increase the second moment of vorticity have been interpreted as having an alleviating effect on the wake.[8] Whether such alleviation is significant depends on the following aircraft weight, span, and encounter trajectory.[2,3]

III. Computational Model

A. Input

The input into the code was the spanwise, normalized, wing-bound vorticity distribution; number of desired wake vortices; and desired output parameters. Within the code, the normalized vorticity distribution was renormalized so that its ratio to a normalized elliptical load would produce the same lift as an elliptically loaded wing (with the same span). This renormalized distribution allowed for comparisons of different distributions, but constrained to the same lift. Further, renormalization using the normalized elliptical load allowed direct scaling of the results to a full-sized airplane given the air density, airplane weight, span, and airspeed. Once specified, the distribution remained constant at the wing, i.e., the wing wake the distribution.

B. Performance Estimations

The load distribution was used directly to compute the nondimensional root bending moment and induced drag. Prandtl-lifting-line methods were used to compute the normalized downwash distribution along the wingspan; this was, in turn, used to compute an estimate of the nondimensional induced drag.[27]

C. Discretized Initial Wake Description

The renormalized bound-vortex distribution was used to generate the system of trailing vortices to be shed from the wing. According to the Helmholtz law of conservation of circulation, the strength of this system of vortices is given as

$$\gamma(y) = \frac{d\Gamma(y)}{dy} \tag{2}$$

$$d\Gamma = -\gamma(y)\, dy \tag{3}$$

where $\gamma(y)$ is the circulation density in the wake at the wing. In the discretized implementation of Eq. (3), the spanwise vorticity distribution $\Gamma(y)$ was first discretized at equal span length locations (unless discretization was sized differently for comparison reasons), determined by the number of vortices chosen for the wake n_y. Equal spacing was used because of the intended use of exploring widely varying distributions without the need for tailoring the spacing to the changing distributions. The streamwise wake-vortex strengths were then set equal to the change in bound vortex strengths at the midpoints between each of the discretization locations. The initial wake emanated at, and in the plane of, the wing, made up of the discretized wake vortices at the spanwise y locations chosen for the discretization. Out-of-wing-plane vortices could also be input with a nonzero z component to analyze the vortex injection schemes.

This initial wake distribution, Γ_i at y_i spanwise locations, was used to compute the center of vorticity at the wing by first computing the semispan circulation, given by

$$\Gamma_0 = -\int_0^{b/2} \gamma(y)\, dy \tag{4}$$

In discretized form, Γ_0 is just the sum of the wake vortex strengths over the semispan:

$$\Gamma_0 = \sum_{i=1}^{n_y/2} \Gamma_i \tag{5}$$

The spanwise center of vorticity was then computed at the wing or at any streamwise position x in discretized form as

$$y_{c.v.} = \left(\frac{1}{\Gamma_0}\right) \sum_{i=1}^{n_y/2} (y_i \Gamma_i) \tag{6}$$

The wing-normal component of the center of vorticity $z_{c.v.}$ was computed by replacing y_i with z_i.

D. Near-Field Wake Dynamics

The present model included the effect of the wing-bound vorticity and the influence of only that part of the wake line vortices emanating at the wing and extending to $x = +\infty$. The in-Trefftz-plane components of induced velocities due to the bound vortex segments were computed via the Biot–Savart law integrated along each segment of the bound vortex based on its distance and position from the particular wake vortex at its location in a Trefftz plane, located at a downstream distance x from the wing. It should be noted that the bound-vortex influence on the wake for most of our studies was computed assuming that the bound vortex was upstream from the trailing edge of the wing a distance of approximately the wing root chord; the rational for this choice was similar to that presented by Moran[28] in describing the lumped-vortex method, and this distance could be adjusted to better approximate the angle that trailing edge of the wing might make to the freestream. At a Trefftz plane a distance x from the wing, the Biot–Savart integration to compute the induced velocities of the wake vortices extended upstream a distance $-x$, and downstream to $+\infty$; thus, at the wing, the induced velocity would be only half that induced by the wake vortices for Trefftz planes located in the far field. The sum of all of the induced velocities (wing-bound and wake) at the location of each wake vortex was then used to displace the vortices in the next Trefftz plane (a distance $V_\infty \Delta t$ downstream) by multiplying the summed velocity by Δt.

E. Rotational Cores and Stability

Finite rotational cores for each discrete vortex were first employed to stabilize calculations by Chorin and Bernard[22] and have been routinely used by other researchers for that purpose since then. In our model, we used the Chorin and Bernard functional form for the cores. Depending on the intended use of the results, core radii of from zero to up to six wing-discretization vortex spacings have been used (in all cases the cores were introduced as linearly expanding radii from zero at the wing to the full specified core radius by $x/s = 0.1$). It should be noted that the introduction of rotational cores is akin to defining the thickness of the viscous shear layer[29]; as such, the larger the cores, the thicker the layer. Thicker layers tend to suppress the smaller-scale Kelvin–Helmholtz instabilities, thereby smoothing the physical roll up; larger cores have the same effect of smoothing the numerical roll up by suppressing the smaller-scale instabilities.[22] Thus, adding the cores tends to smooth the roll up, but such smoothing may or may not mimic the physical situation being modeled. Other effects of adding the cores are discussed in a later section.

F. Asymptotic Dynamics of the Wake

At any Trefftz plane sufficiently far downstream of the wing ($x/b > 2.0$), the wake vortices were treated as line vortices, normal to the Trefftz plane, of strength consistent with that assigned at the wing by the discretization of the spanwise vorticity distribution. The fact that these vortices may have third-dimension curvature was neglected. The induced velocities in the Trefftz plane on each vortex due to the presence of all other vortices in the plane were computed via the Biot–Savart law, and the effect of the bound vortices computed as discussed earlier. These velocities were then used to displace the vortices in the y–z plane by multiplying the induced velocities times

the time step Δt, and translating the new locations in the x direction to the next Trefftz plane a distance $V_\infty \Delta t$ downstream.

G. Wake Descriptors

At any Trefftz plane, the locations of the vortices defined the structure in the wake. Using the vortex strengths and locations, the semispan y and z centers of vorticity were calculated as in Eq. (6). The semispan, second moment was then computed in discretized form as

$$J_2 = \sum_{i=1}^{n_y/2} [(y_i - y_{c.v.})^2 + (z_i - z_{c.v.})^2]\Gamma_i \qquad (7)$$

From which the dispersion radius could be computed as

$$r_D = \sqrt{J_2/\Gamma_0} \qquad (8)$$

IV. Code Validation

A number of studies were done to validate the code by looking at self-consistency measures and by comparing the code's results to results by others using both discrete-vortex and other methods. It is difficult to define accuracy in the usual sense when dealing with discrete-vortex methods because, as has been well documented,[22,23] the use of vortex methods is a tradeoff between spatial resolution, temporal resolution, and numerical stability. Since theoretically, a point vortex has tangential velocities that approach infinity as distance from its center r approaches zero, for a given time step there is a limited distance between vortices that yields any physically meaningful results.[19] This tradeoff between resolution, stability, and meaningful results has been dealt with in many ways, including the introduction of rotational vortex cores[10,22-24] and as simply as decreasing resolution. In our case, we used both limited resolution and, when applicable, included rotational cores.

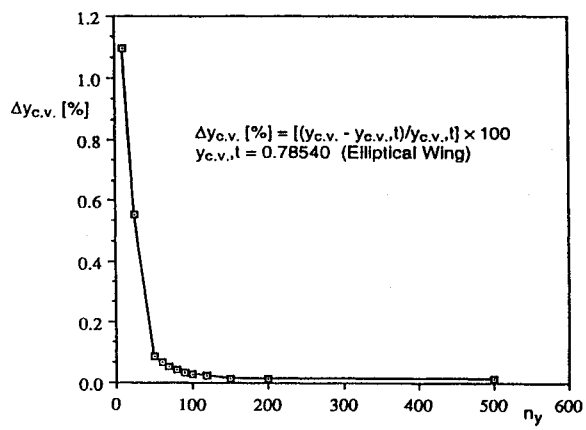

Fig. 1 Relative error in $y_{c.v.}$ vs number of trailing vortices n_y.

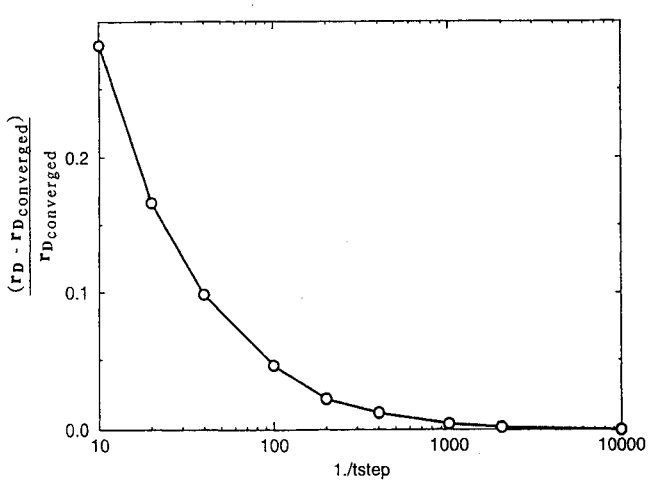

Fig. 2 Relative error in the dispersion radius as a function of time step.

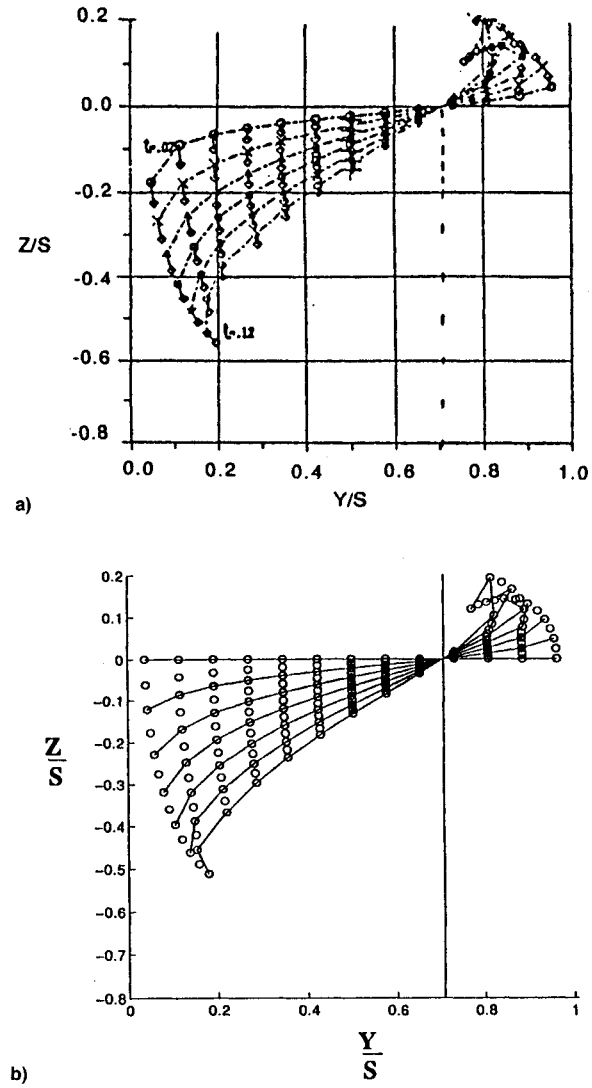

Fig. 3 Comparison of the method by a) Siddiqi[18] with the b) present study for a linearly loaded wing. Times shown in Fig. 3a are related to the nondimensional times of the present study by multiplying by 2π; curves in Fig. 3b are for equivalent times.

A. Resolution

Resolution sufficiency was determined against two criteria: 1) retaining a reasonable time step that maintained numerical stability on the one hand (cf., as discussed later) and 2) the ability to reproduce known analytic solutions on the other. For example, given an elliptic load distribution, it can be shown analytically that the nondimensional, semispan center of vorticity, $\bar{y}_{c.v.}$ (i.e., $y_{c.v.}/s$, where s is the semispan), is located at $\pi/4$. The code was tested over a range of number of vortices n_y to determine how accurately $y_{c.v.}$ was computed. Figure 1 shows the accuracy in computing $\bar{y}_{c.v.}$ compared to the theoretical value $\bar{y}_{c.v.,t}$ as a function of a number of vortices used to describe the wake. For most of our studies 40–60 vortices were used.

B. Time Step

Studies to determine time-step sufficiency can be deceptive; we had initially begun with relatively large time steps and

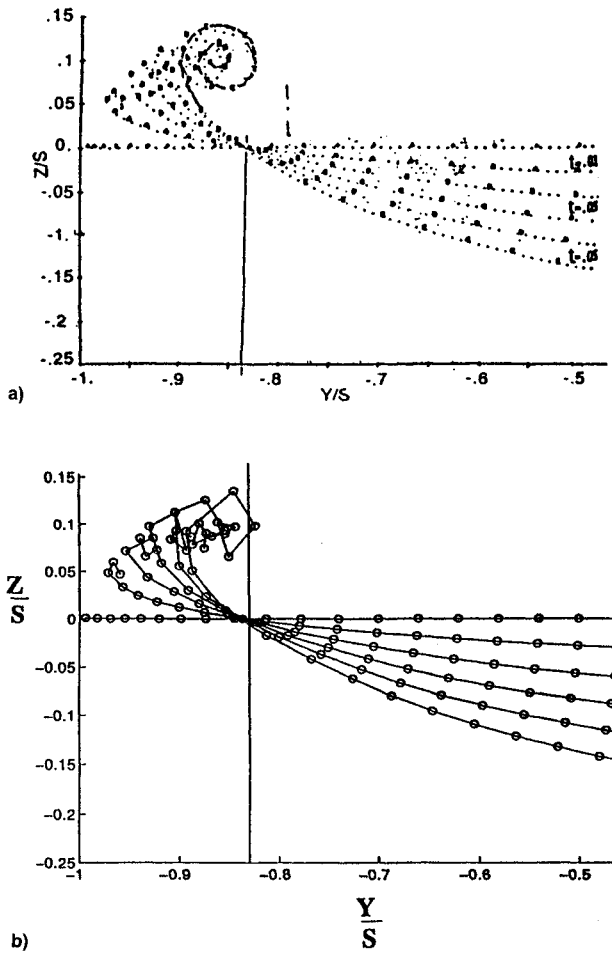

Fig. 4 Comparison of the method by a) Siddiqi[18] with the b) present study for a parabolically loaded wing. Times shown in Fig. 4a are related to the nondimensional times of the present study by multiplying by 2π; curves in Fig. 4b are for equivalent times.

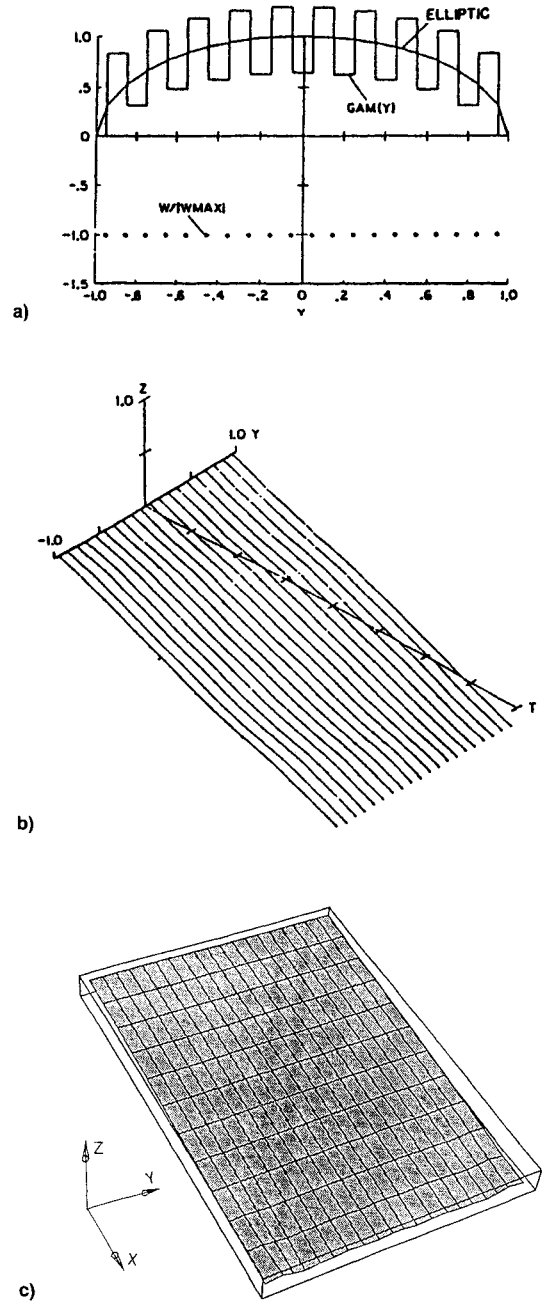

Fig. 5 Comparison of the present method with that by Rossow[20] for a step-span-loaded wing. a) Span loading, b) vortex wake shape, and c) present study.

decreased them until smooth roll ups were obtained. Obtaining smooth roll ups is comparable to satisfying the Westwater criteria referred to by Moore[19]; however, time-step convergence studies illustrated that time-step sizes, sufficiently small to provide smooth roll ups, yet still too large for convergence, had a stabilizing effect on the wake roll up.

Computations of the vortex trajectories from one Trefftz plane to the next assume that the individual induced trajectory from one vortex on another yields a straight path; however, individual induced trajectories should be circular arcs. The larger the time step, the more inaccurate the inferred trajectories become. For an elliptical load, time steps sufficiently small to provide smooth roll ups yet too large for convergence yield dispersion radii computed at successive downstream Trefftz planes that are consistently larger than the time-step converged radii. In effect, this range of time steps introduces a numerical dissipation that tends to diffuse the wake. The dispersion radius for an elliptical load distribution, with no near-wing effects, was computed at $x/s = 4.0$ over a range of nondimensional time steps from 0.1 to 1×10^{-4}. The nondimensional time step is given by

$$\Delta\tilde{t} = \Delta t V_\infty / s \tag{9}$$

A plot of the error in the dispersion radius as a function of nondimensional time step is given in Fig. 2 for $n_y = 50$. The computed dispersion radius from $x/s = 0.0$ to 4.0 at a $\Delta\tilde{t} = 1 \times 10^{-4}$ were compared to calculations by Clemenceau[30] and found to be in excellent agreement. Although most of our studies used a $\Delta\tilde{t} = 1 \times 10^{-3}$ or smaller, because of the roll-up behavior dependence on time step, occasionally care had to be taken to match the time step used by others when comparing results.

C. Comparisons with Other Discrete-Vortex-Method Results

The computed vortex locations in a given Trefftz plane were compared with published results from other discrete-vortex methods; three examples are given in Figs. 3–5. In all of these examples no near-wing effects (wing-bound vorticity and noninfinite vortex wake) were used because the published examples had not incorporated these effects.

It was shown by Siddiqi[18] that the vortex wake generated by a wing with a linear load distribution (in the absence of near-wing effects) rotates around the nondimensional span location $\tilde{y} = \sqrt{2}/2 \approx \pm 0.707$, as shown in Fig. 3a. Successive, time-converged wake contours at the same evolving times computed by the present code are shown in Fig. 3b. Compar-

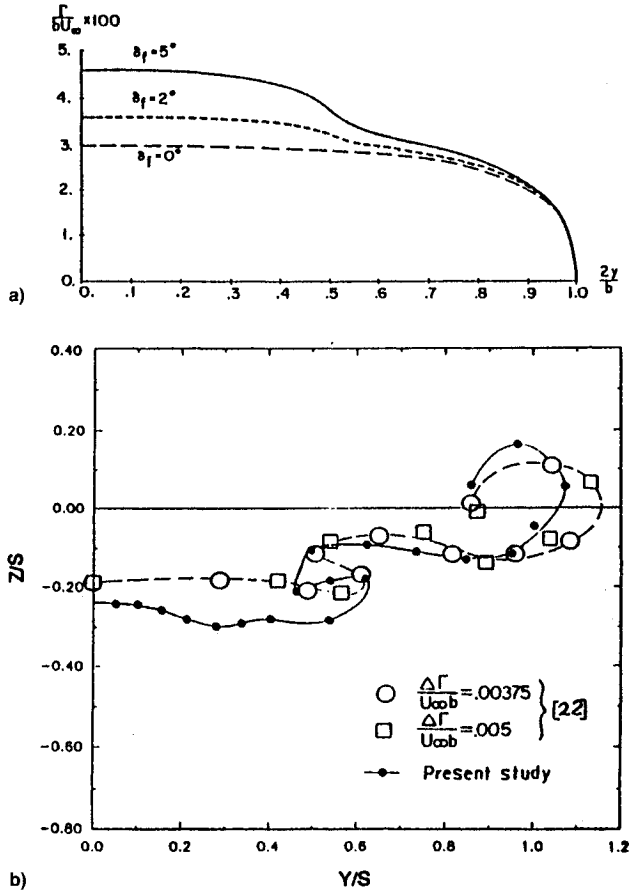

Fig. 6 Comparison of a) the present method (spanwise load distributions) with that by b) Yeh and Plotkin[17] at x/b = 1.69 for a rectangular wing with a 5-deg flap deflection.

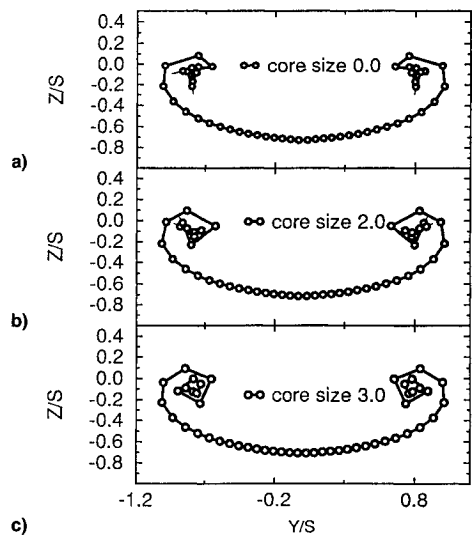

Fig. 7 Trefftz planes computed at x/s = 1.7 using a) no cores, b) core radii equal to two times the initial vortex spacing, and c) core radii equal to three times the initial vortex spacing.

ison between Figs. 3a and 3b show that the rotation position is preserved and wake contours at successive times are in relatively good agreement.

Siddiqi also showed that for a parabolic load distribution (in the absence of near-wing effects) the y intersects of the successive wake contours remain at a fixed spanwise station defined by $\bar{y} \approx \pm 0.84$. Figure 4 compares Siddiqi's results to those of the present code. Siddiqi used 60 vortices to represent the wake with unequal spacing; in the present results the same number of vortices were used; however, only approximately the same unequal spacing was used. As can be seen in Fig. 4, the crossing is preserved and the approximate shape at corresponding times is close to that by Siddiqi.

For the final example, Rossow showed that a stepped-span loading, as shown in Fig. 5a, produces a vortex wake that translates as approximately a planar sheet without undergoing roll up (Fig. 5b, Ref. 20). The wake shape resulting from this load distribution, as generated by the present code neglecting near-wing effects, is shown in Fig. 5c; as in Rossow's results, the wake remained approximately planar. Comparisons of this kind demonstrated that there were no obvious systematic errors in the present code's calculations of the wake.

D. Comparisons with Paneling Codes

Figure 6 shows a comparison of the present code to a computation for a rectangular wing having an AR of 8, clean and with partial flaps deployed at 2 and 5 deg, as computed by Yeh and Plotkin using a vortex panel method.[17] The bound-vortex strength distributions for the clean wing and the two flap settings are shown in Fig. 6a. The results of the present study for an approximation with 40 trailing vortices for a flap deflection of δ_f = 5 deg are shown in Fig. 6b, overlaid with those of Ref. 17. Although not identical, the two are in fair agreement and both capture similar characteristics of the wake roll up. The other two cases (clean wing and δ_f = 2 deg) are not shown here, but were in closer agreement than that for δ_f = 5 deg (Ref. 31). It should be noted that the authors of Ref. 17 specifically state that their method was "limited to calculations with less than one turn of roll up." Consequently, the length of the wake had to be limited to two wingspans; we had no such roll-up limitation, demonstrating, in our mind, that a discrete-vortex method is more properly suited to the study of the wake dynamics than a panel code; on the other hand, the panel code is capable of producing the spanwise load distributions given the wing geometry, a function that vortex methods are incapable of performing.

E. Effect of Rotational Core Size

As mentioned earlier, the effect of adding rotational cores is to stabilize the roll up by suppressing the small-scale instabilities (up to the order of the core radii). While the use of rotational cores changes the details of the rolled up cores, especially in the central region, the use of cores with radii up to six times the wing-discretization distances Δy had only a minor effect on the computed dispersion radii at all streamwise locations. For an elliptically loaded wing discretized using 50 vortices and in the absence of near-wing effects, the computed dispersion radii for core radii of from 0.0 to $6\Delta y$, at x/s = 4.0, differed by less than 0.6%. The effect on smoothing the roll up for the same conditions is demonstrated in Figs. 7a–7c, that show Trefftz planes at x/s = 1.7, with core radii of 0.0, 2.0, and $3.0\Delta y$, respectively. As different as the geometric patterns in the central region of the roll ups are, their dispersion radii are essentially the same. Thus, it can be concluded that a smooth and regular roll up is not required to determine the evolution of dispersion radii.[30]

V. Near-Wing Effects

A. Vertical Trajectories

While the spanwise center of vorticity remains constant with distance downstream from the wing, its out-of-plane, vertical trajectory $z(x)$ does not. Figure 8 shows the computed trajectories for an elliptically loaded wing with and without the effect of the wing-bound vortex and with and without the semi-infinite transition to infinite streamwise vortex filaments. Of these trajectories, only that including the bound vortex yields the trajectory shape observed for actual aircraft, out-of-ground-effect wakes. This shape contains the characteristic that its most rapid descent occurs immediately behind the wing and

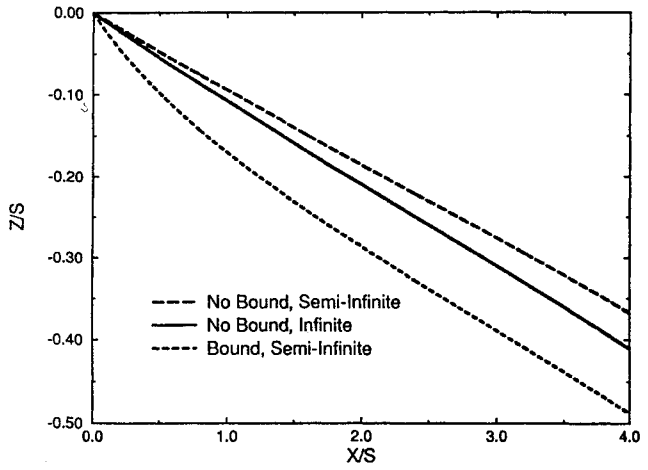

Fig. 8 Vertical trajectory of the wake center of vorticity with no bound vorticity and the wake emanating at $-\infty$, with no bound vorticity and the wake emanating at the wing, and including the effect of the bound vorticity with the wake emanating at the wing.

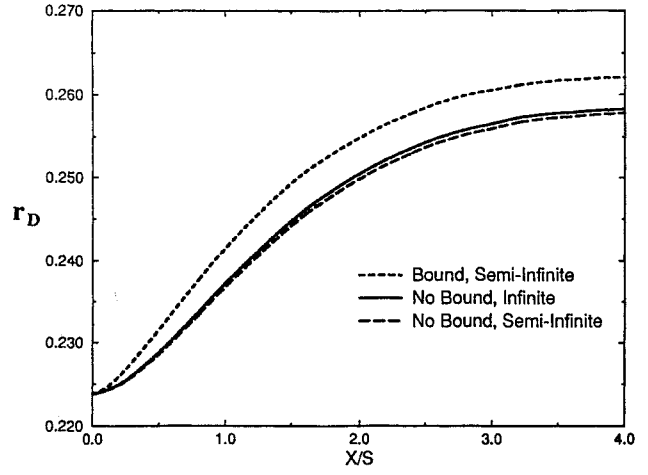

Fig. 9 Development of the dispersion radius with no bound vorticity and the wake emanating at $-\infty$, with no bound vorticity and the wake emanating at the wing, and including the effect of the bound vorticity with the wake emanating at the wing.

settles out to its asymptotic descent rate. As is clear from comparing all three trajectories in Fig. 8, the initial more-rapid descent rate is due to the wing-bound vorticity, with asymptotic descent rate being due to the self-induction rate of the streamwise vortices on each other. As such, the near-wing effects (the wing-bound-vorticity effect in particular) are required to produce the observed characteristic of in-flight, wake trajectories; this implies that near-wing effects should be included in computing the evolution of the wake.

B. Second Moment of Vorticity/Dispersion Radius

Unlike the first moment of vorticity that may be computed at the wing and remains invariant with distance downstream from the wake, the second moment of vorticity changes with position from the wing. Figure 9 shows the evolution of the dispersion radius for an elliptic load distribution out to a distance of $x/s = 4.0$, with and without the effect of the wing-bound vorticity and with and without the semi-infinite transition to infinite streamwise vortex effect. Of the two near-wing effects, it is clear that the least important is the effect of the wake beginning as semi-infinite vortices at the wing. On the other hand, the wing-bound vorticity has a relatively large effect on the development and ultimate disposition of the dispersion radius. It should be noted that the bound-vorticity effect was displaced upstream by 0.5 s (cf., discussed previously, which resulted in an effective angle of attack of approximately 7 deg. Even at this relatively modest effective angle of attack, Fig. 9 shows that the wing-bound vorticity acts to disperse the wake vortices more than predicted if the bound vorticity is neglected.

VI. Conclusions

This article has described a discrete-vortex method for computing the inviscid dynamics of a wake issuing from a lift-producing wing. The method is essentially similar to discrete-vortex methods used by others; however, near-wing effects are included in the present method. The inclusion of wing-bound vorticity and noninfinite-wake effects has been shown to have a relatively large effect on both the vertical trajectory of the wake, and, more importantly, the final disposition of the wake, as shown by the effect on the dispersion radius. Results presented here also demonstrate that a relatively crude discretization of the wake retains good fidelity in describing the wake dynamics within the limitations and approximations of a discrete-vortex method; a reasonable number of wake-representing vortices appears to be from 40 to 60. If smooth roll ups are of interest, rotational cores can be used; however, up to the core sizes studied, use of rotational cores does not appear to effect either the development or the final disposition of the wake dispersion radii. This latter result indicates that smooth, nonchaotic-looking wakes are not necessarily required to study the development of the wake. Studies of time convergence also uncovered the unexpected result that use of time steps sufficiently small to produce smooth-appearing roll ups, but larger than those needed to time converge the solution, introduce a numerical dissipation into the computation. This numerical dissipation has two effects: the first is that roll ups can develop smoothly to relatively large times/distances downstream, that would otherwise have become chaotic in the case of a time-converged solution. Second, this numerical dissipation causes the dispersion radius to continue to grow indefinitely (e.g., in the case of an elliptical load) rather than asymptoting to a constant value. This finding suggests that careful attention must be given to time steps when comparing computed results by other researchers. Finally, it should be mentioned that the present implementation of the discrete vortex method provides an efficient code to investigate large numbers of wing-load distributions; a typical run, using 40 vortices and following the wake development to 10 spans downstream of the wing, requires approximately 3 min on a Sun SPARCstation 5.

Acknowledgments

The authors are greatly indebted to George C. Greene, NASA Langley Research Center, for his many stimulating communications and continual encouragement in our work. The authors would also like to acknowledge the contributions of Vincent E. Pribish.

References

[1]Rossow, V. J., and Tinling, B. E., "Research on Aircraft/Vortex Interactions to Determine Acceptable Level of Wake Intensity," *Journal of Aircraft*, Vol. 25, No. 6, 1988, pp. 481–492.

[2]Nelson, R. C., "Dynamic Behavior of an Aircraft Encountering Aircraft Wake Turbulence," *Journal of Aircraft*, Vol. 13, No. 9, 1976, pp. 704–708.

[3]Stuever, R. A., and Greene, G. C., "An Analysis of Relative Wake-Vortex Hazards for Typical Transport Aircraft," AIAA Paper 94-0810, Jan. 1994.

[4]Olsen, J. A., Goldburg, A., and Rogers, M. (eds.), *Aircraft Wake Turbulence and Its Detection*, Plenum, New York, 1971.

[5]"NASA Symposium on Wake Vortex Minimization," NASA SP-409, 1976.

[6]Hallock, J. N. (ed.), *Proceedings of the Aircraft Wake Vortices Conference*, Federal Aviation Administration, FAA-RD-77-68, March 1977.

[7]Wood, W. D. (ed.), *FAA/NASA Proceedings of the Workshop on the Wake Vortex Alleviation and Avoidance*, Federal Aviation Admin-

the Wake Vortex Alleviation and Avoidance, Federal Aviation Adminration, FAA-RD-79-105, Nov. 1977.

[8]Rossow, V. J., "Prospects for Alleviation of Hazard Posed by Lift-Generated Wakes," *Proceedings of the Aircraft Wake Vortices Conference* (Washington, DC), Vol. 1, DOT/FAA/SD-92/1.1, 1991, pp. 22(1)–22(40).

[9]Betz, A., "Verhalten von Wirbelsystemen," *ZAMM*, Bd. XII, Nr. 3, 1932, pp. 164–174; see also NACA TM 713, June 1933.

[10]Crow, S. C., "Stabililty Theory for a Pair of Trailing Vortices," *AIAA Journal*, Vol. 8, No. 12, 1970, pp. 2172–2179.

[11]Eliason, B. G., Gartshore, I. S., and Parkinson, G. V., "Wind Tunnel Investigation of Crow Instability," *Journal of Aircraft*, Vol. 12, No. 12, 1975, pp. 985–988.

[12]Green, G. C., "Wake Vortex Alleviation," AIAA Paper 81-0798, Jan. 1981.

[13]Green, G. C., Dunham, R. E., Jr., Burnham, D. C., Hallock, J. N., and Rossow, V. J., "Wake Vortex Research Lessons Learned," *Proceedings of the Aircraft Wake Vortices Conference* (Washington, DC), Vol. 1, DOT/FAA/SD-92/1.1, 1991, pp. 2(1)–2(13).

[14]Machol, R., "Opening Remarks," *Proceedings of the Aircraft Wake Vortices Conference* (Washington, DC), Vol. 1, DOT/FAA/SD-92/1.1, 1991, pp. 1(1)–1(10).

[15]Nikolic, V. R., and Jumper, E. J., "Attenuation of Airplane Wake Vortices by Excitation of Far-Field Instability," AIAA Paper 93-3511, Aug. 1993.

[16]Taske, M. E., Quackenbush, R. R., Bilanin, A. J., and Wachspress, D. A., "Vortex Roll-Up Merging and Decay with the Uniwake Computer Program," *Proceedings of the Aircraft Wake Vortices Conference* (Washington, DC), Vol. 1, DOT/FAA/SD-92/1.1, 1991, pp. 33(1)–33(20).

[17]Yeh, D. T., and Plotkin, A., "Vortex Panel Calculation of Wake Rollup Behind a Large Aspect Ratio Wing," AIAA Paper 85-1561, July 1985.

[18]Siddiqi, S., "Trailing Vortex Rollup Computations Using the Point Vortex Method," AIAA Paper 87-2479, Aug. 1987.

[19]Moore, D. W., "A Numerical Study of the Roll-Up of a Finite Vortex Sheet," *Journal of Fluid Mechanics*, Vol. 63, Pt. 2, 1974, pp. 225–235.

[20]Rossow, V. J., "Theoretical Study of Lift-Generated Vortex Wakes Designed to Avoid Rollup," *AIAA Journal*, Vol. 13, No. 4, 1975, pp. 476–484.

[21]Schlichting, H., *Boundary-Layer Theory*, 7th ed., McGraw–Hill, New York, 1979.

[22]Chorin, A. J., and Bernard, P. S., "Discretization of a Vortex Sheet, with an Example of Roll-Up," *Journal of Computational Physics*, Vol. 13, 1973, pp. 423–429.

[23]Sarpkaya, T., "Computational Methods with Vortices—The 1988 Freeman Scholar Lecture," *Journal of Fluids Engineering*, Vol. 111, March 1989, pp. 5–52.

[24]Leonard, A., "Computing Three-Dimensional Incompressible Flows with Vortex Elements," *Annual Review of Fluid Mechanics*, Vol. 17, 1985, pp. 523–560.

[25]Saffman, P. G., *Vortex Dynamics*, Cambridge Univ. Press, New York, 1992.

[26]Rossow, V. J., "On the Inviscid Rolled-Up Structure of Lift Generated Vortices," NASA TM X-62,224, Jan. 1973.

[27]Kuethe, A. M., and Chow, C. Y., *Foundations of Aerodynamics Bases of Aerodynamic Design*, 3rd ed., Wiley, New York, 1976.

[28]Moran, J., *An Introduction to Theoretical and Computational Aerodynamics*, Wiley, New York, 1984.

[29]Ghoniem, A. F., "Vortex Simulation of Reacting Shear Flow," *Numerical Approaches to Combustion Modeling*, edited by E. S. Oran and J. P. Boris, Vol. 135, Progress in Astronautics and Aeronautics, AIAA, Washington, DC, 1990, pp. 305–348.

[30]Clemenceau, J. Y., "On Maximizing the Effect of a Counter-Rotating Vortex on Vortex Sheet Roll-Up Using a Point Vortex Method and a Genetic Optimization Algorithm," M.S. Thesis, School of Engineering and Applied Science, George Washington Univ., Hampton, VA, 1994.

[31]Nikolic, V. R., "A Study of the Development and Attenuation of Wing-Generated, Vortical Wakes," Ph.D. Dissertation, Univ. of Notre Dame, Notre Dame, IN, April 1993.